Cell Reports

Article

Coordinated parieto-frontal neuronal communication is critical for abstract quantity judgments in primates

Graphical abstract

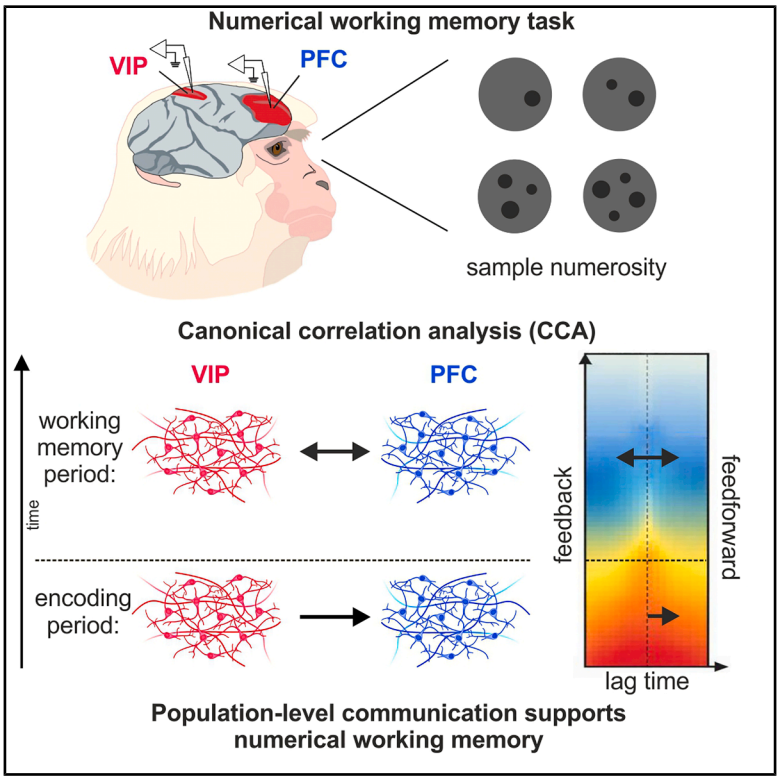

Highlights

- VIP and PFC show dynamic population coupling during numerosity decisions
- Numerosity-selective neurons drive early feedforward signaling from VIP to PFC
- Sustained bidirectional VIP-PFC interactions support numerical working memory
- Error trials show disrupted parieto-frontal communication late in the delay

Authors

Tobias Machts, Andreas Nieder

Correspondence

andreas.nieder@uni-tuebingen.de

In brief

Using simultaneous population recordings and time-lagged canonical correlation analysis in macaques, Machts and Nieder show that numerosity-selective neurons mediate dynamic VIP-PFC communication. Early feedforward signaling supports encoding, whereas sustained bidirectional interactions maintain numerical information. Disrupted parieto-frontal coupling predicts decision errors.

Machts & Nieder, 2026, Cell Reports *45*, 117147
April 28, 2026
https://doi.org/10.1016/j.celrep.2026.117147

CellPress

Cell Reports

CellPress
OPEN ACCESS

Article

Coordinated parieto-frontal neuronal communication is critical for abstract quantity judgments in primates

Tobias Machts[1] and Andreas Nieder[1,2,*]
[1]Animal Physiology, Institute of Neurobiology, University of Tuebingen, Auf der Morgenstelle 28, 72076 Tuebingen, Germany
[2]Lead contact
*Correspondence: andreas.nieder@uni-tuebingen.de
https://doi.org/10.1016/j.celrep.2026.117147

SUMMARY

Accurate numerical cognition relies on representing and comparing quantities, a fundamental skill for adaptive behavior. In nonhuman primates, the parieto-frontal network, including the ventral intraparietal area (VIP) and prefrontal cortex (PFC), supports this process, but the functional dynamics and directionality of communication between these regions remain unclear. We examine population-level interactions of simultaneously recorded neuronal activity between VIP and PFC in two male macaques performing a numerosity task. Using time-lagged canonical correlation analyses, we show that correct trials exhibit sustained correlations driven by numerosity-selective neurons, with early feedforward dominance from VIP to PFC following sample onset. By contrast, error trials show weaker correlations, reduced VIP-to-PFC feedforward signaling, and transient breakdowns during the late working memory period. These findings show that coordinated parieto-frontal population activity enables accurate numerical judgments, whereas disrupted interactions impair performance, highlighting the critical role of dynamic, task-dependent interareal communication in categorical decisions.

INTRODUCTION

Humans and nonhuman animals alike rely on the ability to perceive, represent, and manipulate numerical and quantitative information to navigate their environment. Quantitative categories, such as the number of items in a set, its numerosity, enable essential cognitive functions including foraging, social interactions, and decision-making.[1] The capacity to discriminate and compare quantities underlies more complex mathematical reasoning and problem-solving, making numerical cognition a fundamental aspect of adaptive behavior.[2,3]

The parieto-frontal network, encompassing regions such as the intraparietal sulcus (IPS) in the posterior parietal cortex and prefrontal cortex (PFC), plays a pivotal role in processing numerical information.[4–11] In macaques, neurons within the ventral intraparietal area (VIP) and PFC exhibit tuning to visual numerosity, suggesting a direct encoding of quantity.[12–18] This information subsequently, with a temporal delay, appears in the PFC, where it is integrated with other cognitive processes to support working memory and guide decision-making.[19–22]

Despite known anatomical connections between posterior parietal cortex and PFC,[23,24] the functional connectivity between VIP and PFC, as well as the directionality of information flow, has not been directly tested. The fronto-parietal network provides a flexible communication channel supporting attention, working memory, and decision-making. Previous studies using synchronization measures (e.g., coherence, phase locking, correlation dynamics) have shown that coordinated activity between prefrontal and parietal regions enables integration of sensory evidence with executive control, supporting both bottom-up and top-down processes.[25–30] If parieto-frontal communication is critical for numerical cognition, these interactions should be robust during correct delayed judgments and break down during errors.

We tested and extended this hypothesis in monkeys performing a delayed number-matching task by examining simultaneously recorded parieto-frontal neuron populations using time-lagged canonical correlation analysis (CCA), a dimensionality reduction technique that identifies shared population activity patterns between two brain areas.[31] CCA extracts linear combinations of neuronal activity—canonical dimensions—that are maximally correlated across areas. Unlike traditional synchronization measures, it identifies the specific population subspaces mediating inter-areal communication and, by systematically introducing temporal lags, reveals the structure and directionality of interactions: feedforward signaling occurs when activity in an upstream area precedes correlated activity in a downstream area, and feedback occurs in the reverse direction. We used this approach to investigate how VIP and PFC communicate during numerical judgments, providing new insights into the neural mechanisms of numerical cognition and highlighting the critical role of intact parieto-frontal communication for cognitive performance.

RESULTS

Two rhesus monkeys performed a delayed match-to-sample task in which they matched the number of dots in visual arrays

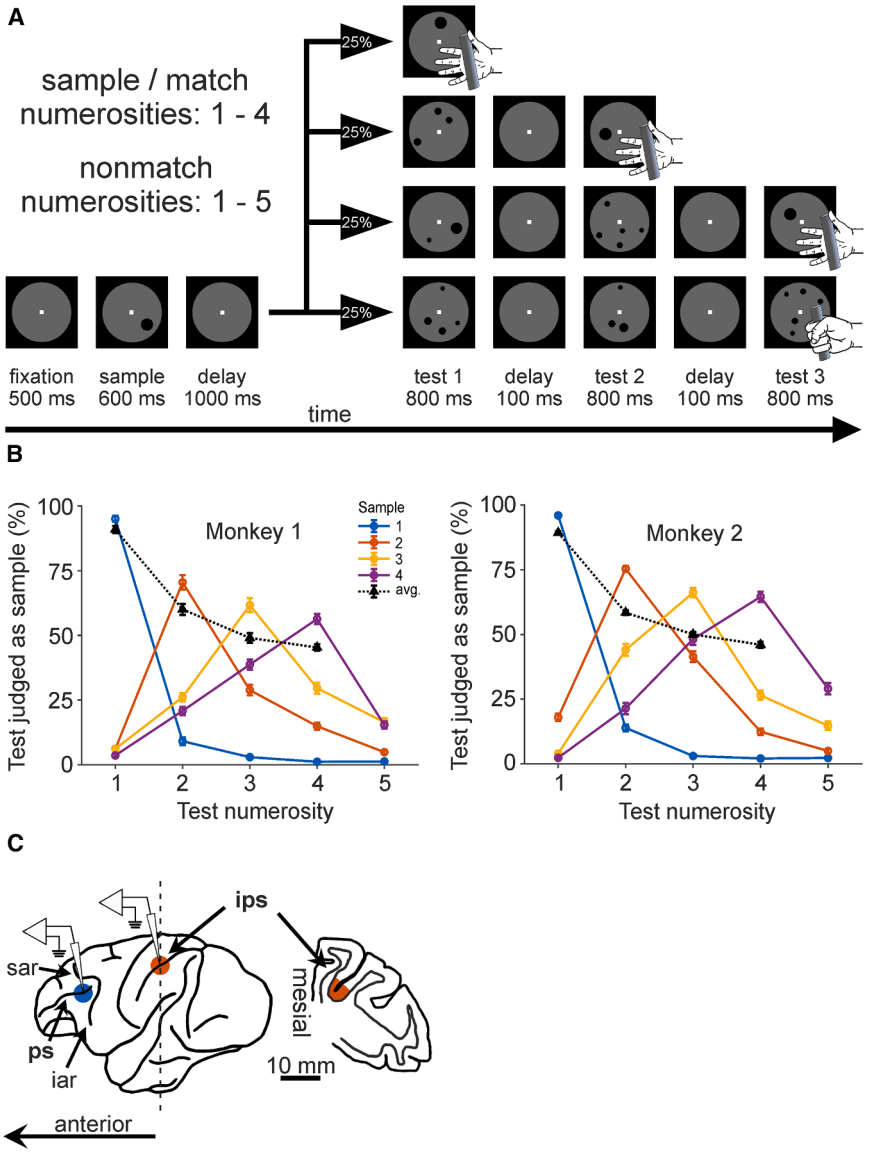

Figure 1. Task protocol, behavioral performance, and recording sites

(A) Monkeys performed a delayed match-to-sample task with dot arrays. Each trial began when the monkey grasped a response bar and maintained fixation on a central target. Sample numerosities (1–4) were presented, followed by a delay period. During up to three sequential test phases (test1–test3), the monkey released the bar for matching numerosities and withheld responding for nonmatching numerosities (1–5). Test phases were pseudo-randomly presented, resulting in four trial conditions. Reproduced from Machts et al.[20]

(B) Behavioral performance of the two monkeys for sample numerosities 1–4. Functions show the probability of judging test displays as matching the sample numerosity (four colors, solid lines). Peaks indicate correct matches, while data points in the flanks reflect errors to nonmatching numerosities. The black dotted line shows the average performance across sample numerosities. Error bars (very small) represent SEM across sessions.

(C) Schematic diagram of the lateral macaque brain showing recording sites in PFC (blue) and VIP (red).

IPS, intraparietal sulcus; PS, principal sulcus; SAR, superior arcuate sulcus; IAR, inferior arcuate sulcus.

(Figure 1A).[20] Sample displays contained 1–4 dots, and test displays contained 1–5 dots. To control for low-level visual features, half of the trials used a standard protocol (dots of random size and location) and half used a control protocol (constant overall dot density and area across numerosities). Each trial began when the monkey grasped a response bar and maintained fixation on a central target. Sample numerosities were presented, followed by a delay period. During up to three sequential test phases (test1–test3), the monkey released the bar for matching numerosities and withheld responding for nonmatching numerosities. Test phases were presented pseudo-randomly, resulting in four trial types, and sample numerosities and trial types were balanced across trials.

Behavioral performance

Both monkeys mastered the task, with mean performance across sessions significantly above chance level of 25% (monkey 1: 27 sessions, 61.32 ± 1.36%, $p < 0.001$; monkey 2: 33 sessions, 60.95 ± 0.58%, $p < 0.001$, Binomial test). To assess their ability to identify the correct matching numerosity, behavioral performance functions were computed for each session, reflecting the probability of judging test numerosities as equal to the sample. For all sample numerosities, both monkeys selected the correct numerosity more frequently than nonmatches and exhibited clear numerical size and distance effects indicative of the approximate number system (Figure 1B).[12,32,33]

Canonical correlation analysis

While the monkeys performed the delayed matching task, we simultaneously recorded neuronal activity in dorsolateral PFC (dlPFC) and VIP of the intraparietal sulcus (60 sessions), brain areas known to represent numerical information.[8] Single-neuron numerosity tuning from this dataset has been reported previously.[20] Here, we focused on analyzing network interactions between VIP and PFC populations.

To investigate population-level interactions, we applied CCA, a dimensionality reduction approach extracting activity patterns in one area that are maximally predictive of activity in the other (Figure 2).[29] To enhance data robustness, we analyzed voltage-thresholded multi-unit activity (MUA) recorded simultaneously from multiple electrodes in PFC and VIP. Of the initial 60 sessions,

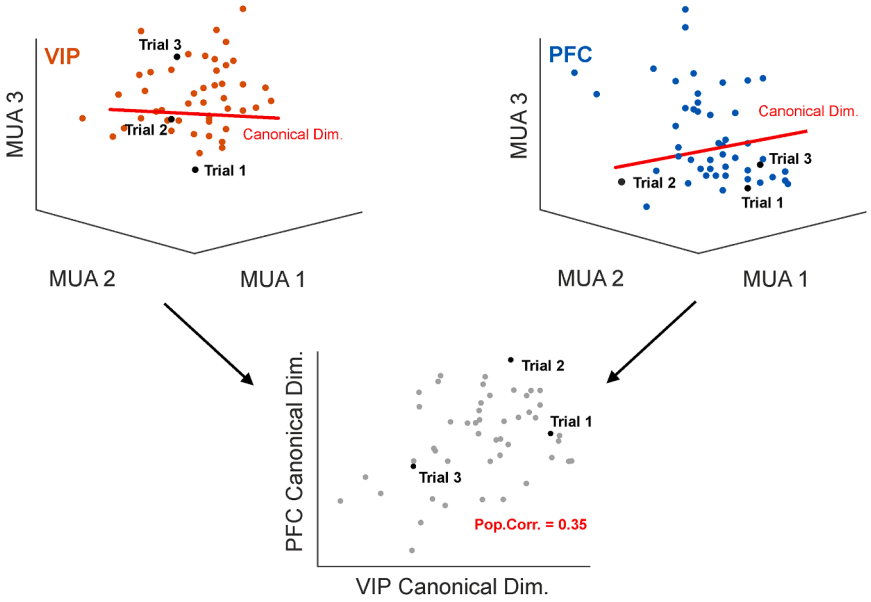

Figure 2. Canonical correlation analysis captures population-level interactions between neurons

In this example, VIP (red, left) and PFC (blue, right) multi-unit activity (MUA) were recorded simultaneously from three electrodes per area. Each circle represents population activity on a single trial; for each VIP activity point, a corresponding PFC point exists. Red axes indicate the first pair of canonical dimensions identified by CCA. Correlating VIP and PFC activity projected onto these dimensions yields a population correlation coefficient (bottom).

After Semedo et al.[29]

we included only those with at least four recording sites per brain area and a minimum of 50 correct and 50 error trials, pooling sessions across numerosities and protocol types (standard vs. control). Using these criteria, 43 sessions were retained for analysis.

To characterize how activity in one area relates to activity in the other across time lags, we applied CCA to population activity vectors from the PFC and VIP, introducing temporal shifts between them.[29] Since these areas are reciprocally connected, with VIP anatomically upstream of PFC, and because prior work shows that neuronal responses and selectivity in VIP lead those in PFC,[17,19,34] we set the maximum time lag to ±40 ms.

We computed a population correlation function (CCA-derived correlation as a function of time lag) across task epochs, from fixation through sample presentation and into the working memory delay. Subsequent Test periods were excluded from analysis due to confounding motor responses. This yielded a two-dimensional population correlation map of the coefficients (Figure 3B).

VIP activity was most strongly correlated with later PFC activity in correct trials

We first examined network interactions based on population correlations during correct trials (Figure 3). Because CCA is sensitive to trial count, we equalized the number of trials across sessions, which allowed us to compute reliable averages (see STAR Methods). Figure 3B shows the average VIP-PFC population correlation map for correct trials.

During the pure fixation period, correlations were absent and did not reach the significance threshold ($p < 0.05$, two-sided; below the 97.5th percentile of the shuffled distribution), indicating chance-level interactions between VIP and PFC. Shortly after sample onset, however, correlation coefficients rose significantly above chance (as indicated by the yellow colors in Figure 3B), with higher values for positive (i.e., VIP leading PFC) than negative lags (right side of the surface plot in Figure 3B). This indicates that VIP activity was most strongly correlated with later PFC activity, consistent with feedforward interaction (until ~200 ms after sample onset). Population correlations remained significant, though lower, until the end of the sample period; however, they did not maintain feedforward dominance during the later phase (400–700 ms). Although correlations declined during the delay, they stayed consistently above chance, indicating ongoing communication between VIP and PFC across time lags throughout the task.

We quantified the lag at which canonical correlations peaked for each time bin using a centroid-based estimation (Figure S1). For each peak, the centroid (center of mass) was computed relative to zero lag to provide a quantitative measure of delays. The centroid was calculated over the range corresponding to the 95th percentile of correlation values around the peak. During the very early sample period, before neurons responded to the stimulus due to their response latency, correlation maxima were near zero lag. Once response latency was exceeded and neurons became active, the maxima shifted systematically toward positive lags, peaking around +10 ms, consistent with feedforward dominance from VIP to dlPFC. At the sample-to-delay transition, correlation maxima returned near zero and remained centered throughout the delay, indicating balanced bidirectional coupling without a consistent lead-lag relationship.

VIP dominance at the onset of the sample

We addressed feedforward and feedback projections functionally by analyzing the direction and structure of correlated population activity across time lags. Feedforward interactions were defined as stronger correlations when VIP led PFC (positive lags), whereas feedback interactions were defined as stronger correlations when PFC led VIP (negative lags). These analyses were performed across different task epochs (fixation, sample, and delay), and first for correct trial conditions.

To quantify VIP-PFC communication directionality, we calculated the area under the positive-lag curve ($AUC_{feedforward}$, Figure 3C) as a measure of VIP-to-PFC feedforward correlation, and the area under the negative-lag curve ($AUC_{feedback}$, Figure 3A) for PFC-to-VIP feedback, using a sliding-window approach at each time step (see STAR Methods). Both

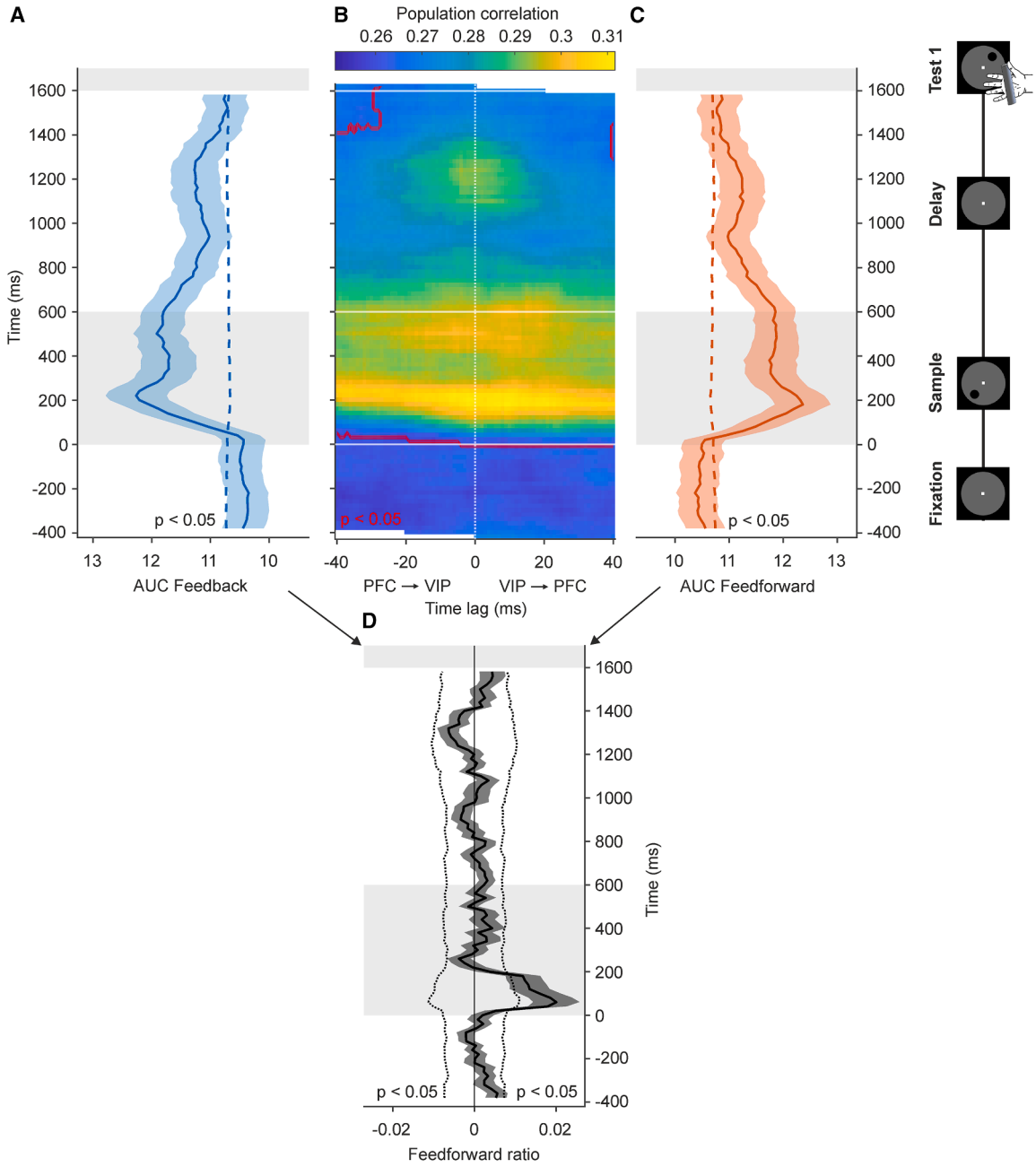

Figure 3. VIP-PFC interactions for correct trials

(A) The area under the feedback sides (AUC, negative lag, PFC → VIP) of the population correlation map (from (B), left half) is shown for correct match trials at all time points. Time 0 is the onset of the sample stimulus, indicated by the gray shaded area. The colored shaded area indicates SEM ($N = 43$ sessions). The dashed horizontal line depicts the significance threshold, which is set to $p < 0.05$ (two-sided).

(B) Averaged population correlation coefficients at all trial times and lag times during correct match trials ($N = 43$ sessions). The horizontal axis represents the time lag between brain areas ($t_1 - t_2$), and the vertical axis represents time relative to sample onset. White horizontal lines indicate the duration of the fixation, sample, delay, and test1 periods. The dashed vertical line indicates zero-lag population correlations ($t_1 = t_2$; see Figure S1A). White areas denote times for which population correlations could not be computed; that is, the PFC activity window had reached either the beginning or the end of the trial. The red boundary indicates the significance threshold, which was set to $p < 0.05$ (two-sided).

(C) Area under the feedforward sides (AUC, positive lag, VIP → PFC) of the population correlation map (from (B), right half) for correct match trials at all time points. Same layout as in (A).

(D) Feedforward ratio at all time points for correct trials. The feedforward ratio is defined as the difference between the areas under the feedforward (positive lag, (A)) and feedback (negative lag, (C)) sides of the population correlation function, divided by their sum. Shaded area indicates SEM ($N = 43$ sessions). The dashed vertical lines indicate the significance threshold set to $p < 0.05$ (two-sided).

feedforward and feedback AUC values remained significantly above chance from sample onset through the end of the delay period.

To quantify directional dominance—whether communication was *more* feedforward or *more* feedback—we contrasted $AUC_{feedforward}$ and $AUC_{feedback}$ and computed a feedforward ratio (Figure 3D). The feedforward ratio is defined as the difference between the area under the positive-lag curve ($AUC_{feedforward}$; Figure 3C) and the area under the negative-lag curve ($AUC_{feedback}$; Figure 3A), divided by their sum at each time step (see STAR Methods).

Significant VIP dominance emerged shortly after sample onset (0.018 ± 0.005; 97.5th percentile: 0.010) and persisted until ~200 ms (0.012 ± 0.004; 97.5th percentile: 0.009), indicating predominantly feedforward communication from VIP to PFC. Beyond this window, neither area showed significant directional dominance during the later sample period or the subsequent delay.

Main interaction patterns were qualitatively consistent across animals. In both monkeys, VIP^{-}dlPFC correlations were strongest during the sample period, showing transient feedforward VIP-to-dlPFC dominance around stimulus onset, followed by balanced bidirectional coupling during the delay (Figure S2). Correlation magnitudes varied, but the temporal structure and directionality were similar across subjects.

Inter-areal communication specific to numerical information

To test whether the observed inter-areal communication was specific to numerical information rather than reflecting nonspecific recurrent or bidirectional dynamics, we repeated the canonical correlation analysis as a function of neuronal numerosity selectivity (Figure 4). Each recording site was categorized as numerosity sample-selective, numerosity delay-selective, or numerosity unselective using a one-way ANOVA with the factor numerosity (1–4; $p < 0.01$).[20] Note that some MUAs were selective during both the sample and delay periods.

Across VIP and dlPFC, the majority of recording sites showed numerosity selectivity during either the sample or delay period (VIP: 151/257; dlPFC: 205/270), whereas a smaller fraction did not exhibit task-related selectivity (VIP: 106/257; dlPFC: 65/270). The distribution of selectivity classes across cortical areas is shown in Figure 4D.

Inter-areal population correlations were driven by numerosity-selective units. Correlations were strongest for sample-selective MUAs (Figure 4A), followed by weaker VIP-dlPFC correlations for delay-selective MUAs. (Figure 4B) In contrast, correlations were virtually absent for non-selective MUAs (Figure 4C). Feedforward directionality for numerosity-selective neuron groups was similar.

To further quantify the contribution of task-selective neuronal populations to inter-areal coordination, we computed mean population correlation values across time lags for each selectivity class (Figure 4E). Sample-selective MUAs showed significantly higher mean population correlation values than non-selective MUAs during sample presentation and the subsequent delay period ($p < 0.05$, Mann-Whitney U test, two-sided). Mean correlation values for delay-selective MUAs were lower overall but did not differ significantly from those of sample-selective MUAs.

Importantly, weaker inter-areal correlations in non-selective MUAs cannot be explained by population size. In VIP, where selectivity groups were similar in number (Figure 4D), non-selective MUAs still showed markedly lower correlations. Delay-selective MUAs also exceeded non-selective correlations despite comparable numbers. Overall, these results indicate that VIP-dlPFC communication is specific to numerical information, rather than reflecting nonspecific recurrent or bidirectional dynamics.

Interaction breakdown in error trials during the late delay period

Next, we analyzed balanced numbers of error trials from the same sessions. Error trials were defined exclusively as incorrect behavioral decisions, namely failures to release the bar on match trials or erroneous releases on non-match trials. Trials with fixation breaks, premature responses, or aborted trials were excluded from all analyses.

Figure 5B shows the average VIP-PFC population correlation map for error trials. As in correct trials, correlations during fixation remained below significance ($p < 0.05$, two-sided; below the 97.5th percentile of the shuffled distribution). Shortly after sample onset, correlation coefficients rose significantly above the 97.5th percentile of the shuffled distribution. Correlations were higher for positive than negative lags, indicating again feedforward dominance (VIP leading PFC) after sample onset. Subsequently, correlations were balanced on the positive and negative lag sides, eliminating clear lag dominance. This balance between positive and negative lags persisted throughout the delay period. Notably, in error trials, population correlations dropped below chance at the end of the delay for both positive and negative lags (Figure 5B), whereas correlations in correct trials remained consistently above the significance threshold ($p < 0.05$; Figure 3B).

Interaction differences between correct and error trials

We examined the relative differences (percentage change) in canonical correlation values between correct and error trials for each monkey (Figure S3). In both animals, correlations were higher for correct trials near the end of the sample period and during the late delay. While the magnitude of these differences varied across monkeys, the temporal profile and direction of correct-error modulation were consistent. These results indicate that the reduction of inter-areal coupling during error trials is a reliable phenomenon across subjects.

Next, we compared overall correlation strength between correct and error trials. We computed the percent difference between the population correlation maps of correct and error trials (Figure 6A). No differences were present in the pure fixation period. However, significant correlation differences emerged for positive time lags at the beginning of the sample period and for all time lags exceeding 10% at the end of the sample and the end of the delay period. Statistical significance was confirmed with a binwise two-sided Wilcoxon signed-rank test, indicated on the map in Figure 6A by a red line ($p < 0.05$).

To complement this analysis, we calculated a mean population correlation function, averaging correlations across all time

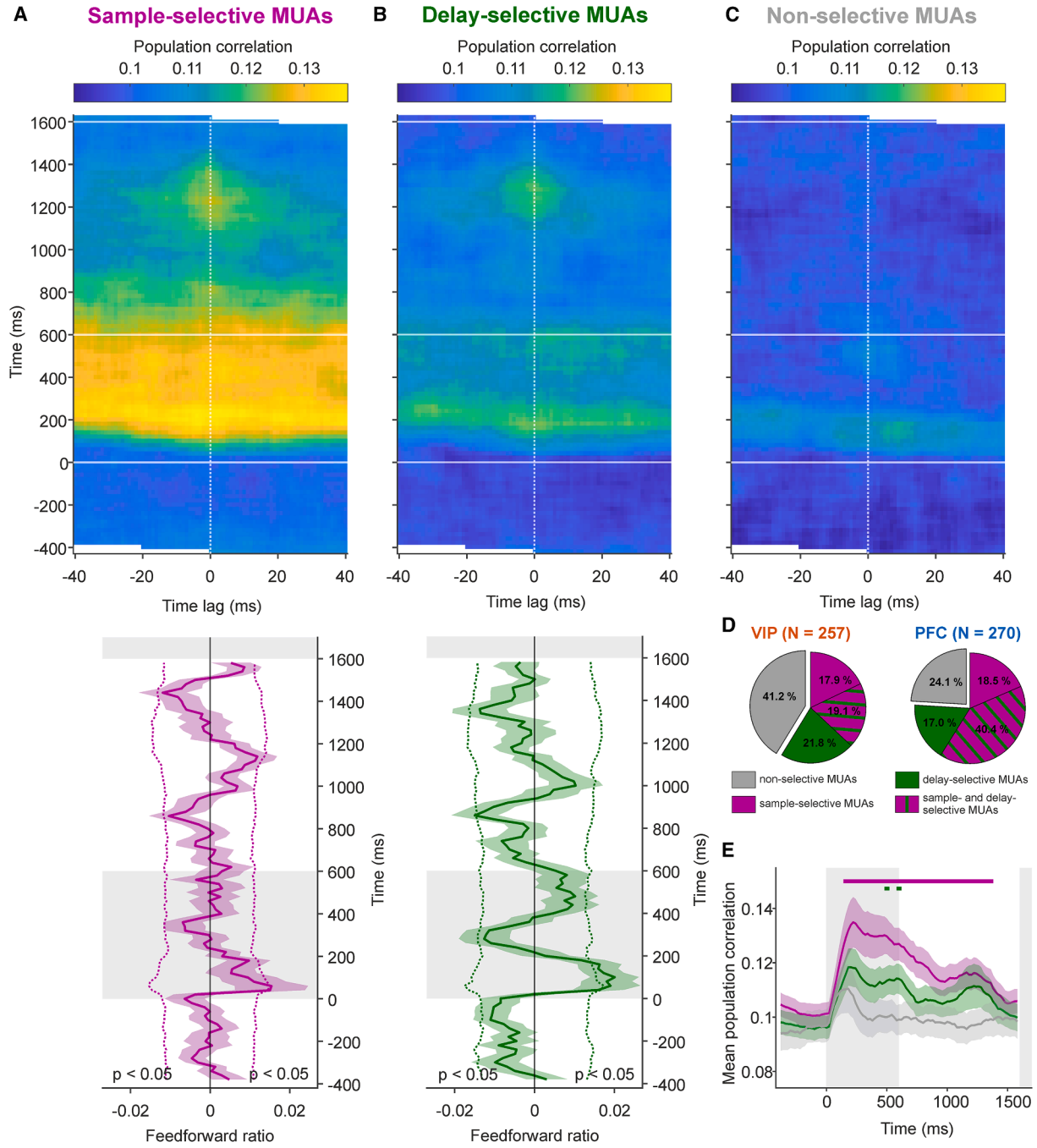

Figure 4. Numerosity-selective neuronal populations contribute to VIP-dlPFC population correlations

(A) Averaged population correlation coefficients across all trial and lag times for sample-selective MUAs. Analyses include correct trials only. Layout matches Figure 3B. The corresponding feedforward ratio at all time points is shown at the bottom.

(B) Averaged population correlation coefficients across all trial and lag times for delay-selective MUAs. Layout as in (A).

(C) Averaged population correlation coefficients across all trial and lag times for non-selective MUAs. Layout as in (A).

(D) Distribution of task-selective MUAs in VIP and dlPFC. Pie charts show the proportion of sample-selective, delay-selective, and non-selective MUAs in VIP (*left*) and dlPFC (*right*). Some MUAs were selective in both periods (dashed shading). Non-selective MUAs showed no significant modulation in either epoch.

(E) Mean time-resolved population correlations for correct trials, shown by selectivity class: sample-selective (magenta), delay-selective (green), and non-selective (gray). Mean correlations represent the average across all time lags between brain areas ($t_1 - t_2$). Time 0 corresponds to sample onset. The magenta bar at the top marks time bins where sample-selective MUAs differ significantly from non-selective MUAs ($p < 0.05$, two-sided Mann-Whitney U test). The green bar at the top marks time bins where delay-selective MUAs differ significantly from non-selective MUAs ($p < 0.05$, two-sided Mann-Whitney U test). Dark shading indicates SEM.

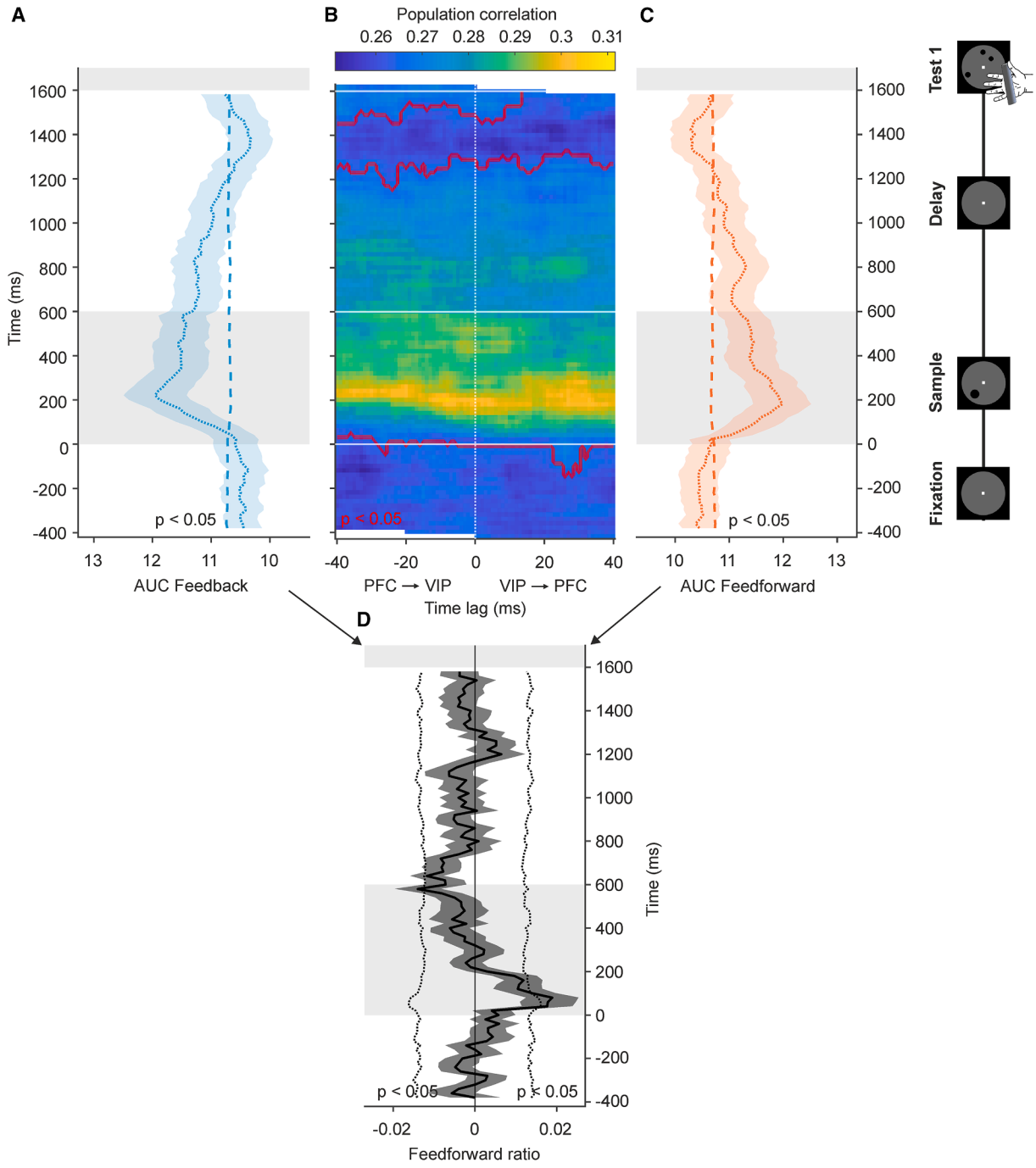

Figure 5. VIP-PFC interactions for error trials

(A) The area under the feedback sides (AUC, negative lag, PFC → VIP) of the population correlation map (from (B)) is shown for error trials at all time points. Time 0 is the onset of the sample stimulus, indicated by the gray shaded area. The colored shaded area indicates SEM ($N = 43$ sessions, same sessions and scaling as in Figure 3). The dashed horizontal line depicts the significance threshold, which is set to $p < 0.05$ (two-sided).

(B) Averaged population correlation coefficients at all trial times and lag times during error trials ($N = 43$ sessions, same sessions and scaling as in Figure 3). The dashed vertical line indicates zero-lag population correlations ($t_1 = t_2$, see Figure S1B). Same layout as in Figure 3B.

(C) The area under the feedforward sides (AUC, positive lag, VIP → PFC) of the population correlation map (from (B)) for error trials at all time points. Same layout as in (A).

(D) Feedforward ratio at all time points for error trials. Same layout as in Figure 3D.

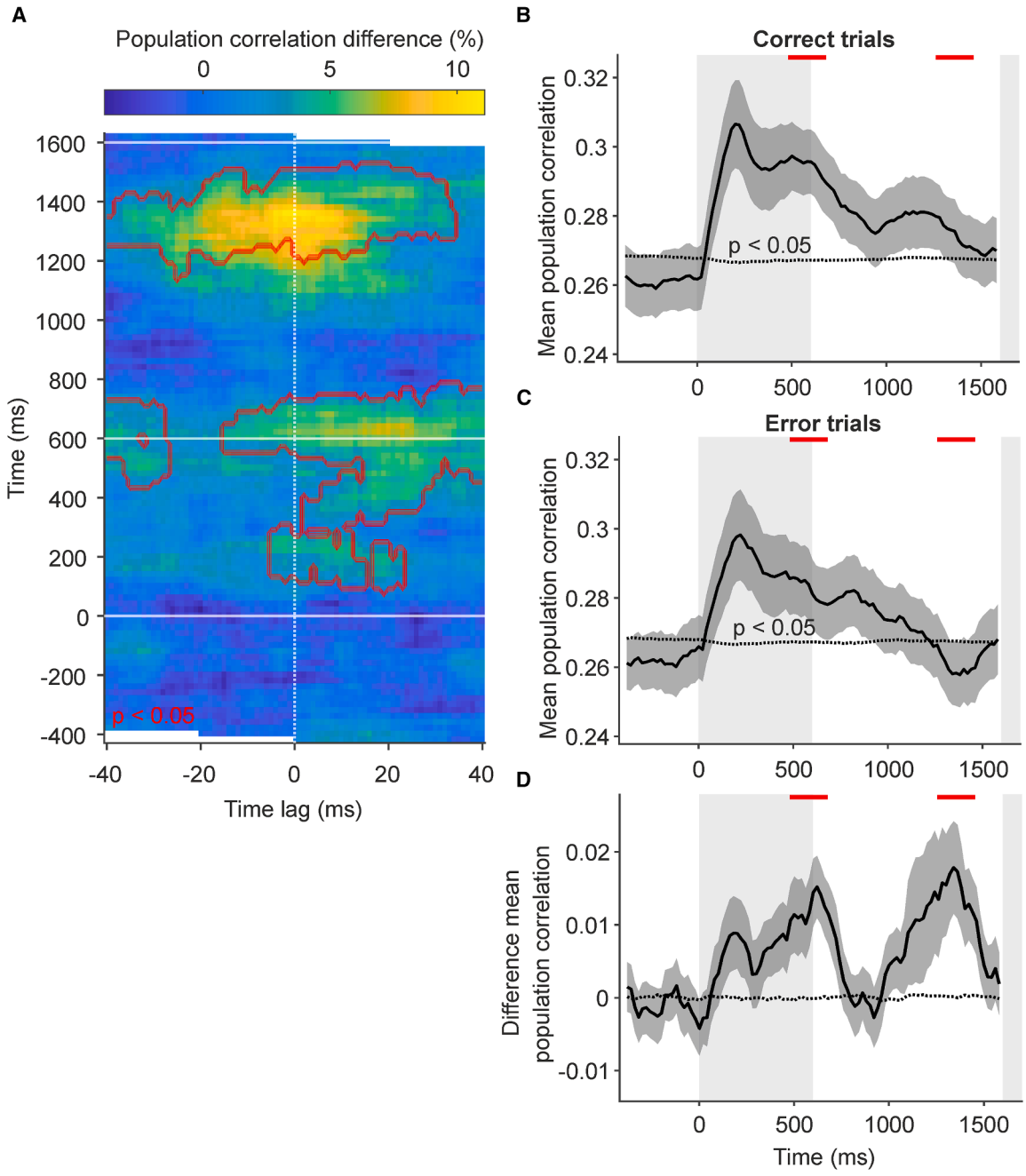

Figure 6. VIP-PFC interaction differences between correct and error trials

(A) The difference in percent between the population correlation coefficient maps of correct and error trials ($N = 43$ sessions, from Figures 3B and 5B). Same layout as in Figure 3B. The red boundary indicates the results of the bin-wise Wilcoxon signed-rank test ($p < 0.05$, two-sided).

(B) Mean time-resolved population correlations for correct trials. The mean population correlation refers to the average of all population correlations across all time lags between brain areas ($t_1 - t_2$). Time 0 is the onset of the sample stimulus indicated by the gray shaded area. The dark shaded areas indicate SEM ($N = 43$ sessions). The dashed horizontal line depicts the significance threshold set to $p < 0.05$ (two-sided). Red bars on the top of the subplot indicate significant differences between the mean correlation coefficients per time bin for error trials ((C), $p < 0.05$, Wilcoxon signed-rank test, two-sided).

(C) Mean population correlations for error trials. Red bars on the top of the subplot indicate significant differences between the mean correlation coefficients per time bin for correct trials ((B), $p < 0.05$, Wilcoxon signed-rank test, two-sided). Same layout as in (B).

(D) The absolute difference between the mean population correlations of correct and error trials ($N = 43$ sessions, from (B) and (C)). The dashed horizontal line depicts the difference between the shuffled distributions of correct and error trials. Same layout as in (B).

lags between brain areas (−40 to +40 ms). These functions were computed separately for correct (Figure 6B) and error trials (Figure 6C) and compared using a binwise two-sided Wilcoxon signed-rank test. Consistent with previous results, correlations were significantly higher in correct trials at the end of the sample presentation (500–680 ms) and during the later delay phase (1260–1440 ms). The difference between the two functions (correct − error) and the significant difference periods are shown in Figure 6D. A similar picture emerged for zero-lag population correlations in correct and error trials (Figure S4). These results indicate that stronger and sustained VIP-PFC population correlations, particularly at the end of the sample and delay periods, are associated with correct numerical judgments, whereas weakened or disrupted correlations characterize error trials.

DISCUSSION

In this study, we examined how neuronal populations in VIP and dlPFC interact during numerical working memory using CCA. Our results show that parieto-frontal communication is dynamic and task-dependent: during stimulus presentation, VIP activity predicted later PFC activity, consistent with a feedforward influence. This early dominance transitioned into balanced bidirectional communication, which persisted across the delay period. Inter-areal population correlations were driven almost exclusively by numerosity-selective neurons, particularly sample-selective units and, to a lesser extent, delay-selective units. In contrast, non-selective MUAs showed negligible correlations across time lags. These results indicate that the reported inter-areal communication is specific to numerical information, rather than reflecting nonspecific recurrent or bidirectional dynamics related to attention or task engagement. Critically, the strength and persistence of these correlations distinguished correct from error trials, suggesting that intact VIP-PFC interactions are necessary for accurate numerical judgments.

Population-level insights with CCA

By using CCA, we were able to reveal population subspaces that mediate VIP-PFC communication, going beyond traditional synchronization measures. Most previous studies of fronto-parietal communication have relied on synchronization measures (e.g., coherence, phase locking, or correlation dynamics) to characterize large-scale coupling between brain regions.[23–28] These approaches demonstrate that oscillatory coupling and spike-field coherence carry task-relevant information and reflect the balance of top-down and bottom-up signaling. However, such measures typically assess coupling at the level of individual electrodes, frequency bands, or spike-field relations, without directly probing the population activity subspaces through which feedforward and feedback signals are exchanged.

By contrast, Semedo et al.[29] introduced a dimensionality reduction framework based on CCA that extracts the population-level patterns of activity in one area that are maximally predictive of activity in another. Crucially, they showed that feedforward and feedback interactions recruit different, largely orthogonal subspaces of population activity, implying that information is routed via distinct channels depending on interaction direction. Applying this method to parieto-frontal circuits extends prior work[35] by moving beyond simple synchronization strength to reveal how population-level communication is structured, temporally directed, and functionally segregated between feedforward and feedback signals.

Feedforward dominance at stimulus encoding

The transient feedforward dominance from VIP to PFC shortly after sample onset aligns with anatomical and physiological evidence that the intraparietal sulcus provides an initial source of numerical information to prefrontal cortex.[17] The feedforward lags are consistent with physiological conduction delays. The ∼10 ms VIP response lead over dlPFC after presentation of numerosity stimuli aligns with our previous findings of +11 ms (Figure 9 in Merten et al.[32]) and +13 ms (Figure S6 in Jannasch et al.[33]). Similar feedforward dynamics have been observed for perceptual and attentional signals in parieto-frontal networks.[23,26] Our findings suggest that numerical information is initially extracted in parietal cortex and transmitted to PFC for further evaluation and integration into working memory representations.

Recurrent parieto-frontal loops during maintenance

After the initial feedforward phase, correlations remained significant but showed no consistent dominance of VIP or PFC. This balance suggests that working memory relies on recurrent communication between parietal and prefrontal cortex rather than exclusively on PFC maintenance mechanisms.[19] This view is supported by models of distributed working memory, which propose that prefrontal activity is stabilized and reinforced through reciprocal interactions with posterior cortical regions.[28,36–38] Our findings provide direct evidence at the population level that recurrent VIP-PFC interactions support the maintenance of numerical information over memory delays.

Breakdown of communication in error trials

A key finding is that error trials were associated with a breakdown of VIP-PFC correlations at the end of the delay, a phase critical for transforming maintained representations into decision signals. This disruption suggests that errors arise not merely from weak tuning within areas but from failures in interareal coordination. Similar communication failures have been reported in parieto-frontal networks during attentional lapses[27] and impaired decision-making,[24] pointing to a general mechanism whereby weakened long-range interactions undermine cognitive control and task performance.

Implications for numerical cognition and dyscalculia

These results extend current models of numerical cognition by demonstrating that accurate number judgments require not only numerosity-selective neurons but also intact communication between parietal and prefrontal populations. The observed breakdown of communication in error trials suggests that numerical deficits, whether transient or chronic, may partly reflect impaired fronto-parietal interactions.

Our findings of disrupted or weakened VIP-PFC interactions during errors resonate with evidence from children with developmental dyscalculia, where atypical parieto-frontal connectivity has been consistently reported. Structural and functional

imaging studies show that children with dyscalculia exhibit altered connectivity within numerical brain networks, including both hyperconnectivity during arithmetic tasks[39] and abnormal anatomical graph-theoretical properties.[40] Importantly, these aberrant connectivity patterns are not static: targeted numerical interventions can normalize functional hyperconnectivity,[41] and more recent work demonstrates altered effective connectivity specifically in dyscalculic children.[42] Longitudinal evidence further suggests that mathematical learning deficits originate from atypical development of a fronto-parietal brain network early in childhood.[43] Taken together, these human data align with our observation that successful task performance depends on strong and sustained VIP-PFC communication, supporting the idea that disrupted fronto-parietal interactions constitute a core neural mechanism underlying both transient errors in primates and persistent numerical learning difficulties in humans.

Current treatments for developmental dyscalculia rely largely on extensive behavioral training, often with limited success. A macaque model could provide a valuable platform for testing pharmacological interventions aimed at strengthening network connectivity. Both the parietal association cortex and the dorsolateral prefrontal cortex (dlPFC) rely heavily on neuromodulatory mechanisms. For example, activation of muscarinic M1 receptors (M1Rs) enhances dlPFC circuit function by modulating neuronal excitability through KCNQ potassium channels. This mechanism supports working memory in primates.[44] Cholinergic modulation likely interacts with other neuromodulatory systems, including dopamine and norepinephrine. These systems also shape dlPFC persistent activity and network stability.[45–47] Although speculative, M1R agonists such as *xanomeline* may enhance VIP-dlPFC communication. The macaque model might be suitable for testing such interventions.

Limitations of the study

A limitation of our study is that time-lagged canonical correlation analysis does not provide direct evidence of causal information flow between VIP and dlPFC. The observed temporal asymmetries are consistent with feedforward VIP-to-dlPFC communication but could in principle also arise from a third area projecting to both regions with different delays. For instance, neurons in the medial temporal lobe of humans, such as parahippocampal area and hippocampus, also contain numerosity-selective neurons.[48–50] While VIP-dlPFC interactions carry numerical information, future studies using causal manipulations, such as targeted inactivation or optogenetic perturbation, are needed to establish the functional influence of VIP on dlPFC.

We note that time-lagged canonical correlation analysis benefits from large simultaneously recorded populations, whereas our recordings included an average of 6.0 ± 0.2 sites in VIP and 6.3 ± 0.2 sites in dlPFC per session (43 sessions total). All analyses were based on multi-unit activity, which pools spiking from multiple neurons per electrode and increases robustness. The relatively modest population size may contribute to the lower canonical correlation values (~0.3) compared to larger-scale tCCA studies (e.g., Semedo et al., 2022).[29] Nevertheless, the temporal structure, task selectivity, and inter-areal patterns were consistent across sessions and animals, supporting the validity of our conclusions.

Future work should test causal links between parieto-frontal communication and numerical behavior using perturbation methods or causal modeling. Extending this work to developmental trajectories will also be critical, as fronto-parietal connectivity supporting numerical cognition emerges gradually during childhood and undergoes refinement with learning.[41] Bridging primate neurophysiology with human neuroimaging could help identify conserved network mechanisms and, in turn, inform interventions for disorders such as developmental dyscalculia. More broadly, our approach illustrates how analyzing population-level communication between higher cortical areas can reveal principles of cognitive control and working memory that generalize beyond numerosity processing.

RESOURCE AVAILABILITY

Lead contact

Further information and requests for resources and reagents should be directed to and will be fulfilled by the lead contact, Andreas Nieder (andreas.nieder@uni-tuebingen.de).

Materials availability

This study did not generate new unique reagents.

Data and code availability

- Processed data are publicly available at https://doi.org/10.6084/m9.figshare.31235425.
- Original analysis code is publicly available and provided at https://doi.org/10.6084/m9.figshare.31235425.
- Any additional information required to reanalyze the data reported in this paper is available from the lead contact upon request.

ACKNOWLEDGMENTS

This research was supported by DFG grants NI 618/15-1 and NI 618/17-1 (FOR 5159).

AUTHOR CONTRIBUTIONS

T.M. and A.N. designed the experiment, T.M. recorded the data, T.M. and A.N. analyzed the data, T.M. and A.N. wrote the paper, and A.N. supervised the study.

DECLARATION OF INTERESTS

The authors declare no competing interests.

DECLARATION OF GENERATIVE AI AND AI-ASSISTED TECHNOLOGIES IN THE WRITING PROCESS

The authors used ChatGPT, developed by OpenAI, for language editing assistance in this manuscript. ChatGPT was solely utilized for language proofreading purposes and did not contribute to or influence any intellectual content within the manuscript.

STAR★METHODS

Detailed methods are provided in the online version of this paper and include the following:

- KEY RESOURCES TABLE
- EXPERIMENTAL MODEL AND PARTICIPANT DETAILS
  - Subjects
- METHOD DETAILS
  - Experimental apparatus and stimuli

SUPPLEMENTAL INFORMATION

Supplemental information can be found online at https://doi.org/10.1016/j.celrep.2026.117147.

Received: October 10, 2025
Revised: February 3, 2026
Accepted: February 27, 2026

REFERENCES

1. Nieder, A. (2020). The Adaptive Value of Numerical Competence. Trends Ecol. Evol. *35*, 605–617.
2. Nieder, A. (2025). The calculating brain. Physiol. Rev. *105*, 267–314.
3. Nieder, A. (2026). The making of number: from content to representation. Trends Cogn. Sci. *S1364–6613*, 00360-2. https://doi.org/10.1016/j.tics.2025.12.011.
4. Sawamura, H., Shima, K., and Tanji, J. (2002). Numerical representation for action in the parietal cortex of the monkey. Nature *415*, 918–922.
5. Dehaene, S., Piazza, M., Pinel, P., and Cohen, L. (2003). Three parietal circuits for number processing. Cogn. Neuropsychol. *20*, 487–506.
6. Piazza, M., Izard, V., Pinel, P., Le Bihan, D., and Dehaene, S. (2004). Tuning curves for approximate numerosity in the human intraparietal sulcus. Neuron *44*, 547–555.
7. Nieder, A. (2004). The number domain- can we count on parietal cortex? Neuron *44*, 407–409.
8. Nieder, A., and Dehaene, S. (2009). Representation of number in the brain. Annu. Rev. Neurosci. *32*, 185–208.
9. Nieder, A. (2016). The neuronal code for number. Nat. Rev. Neurosci. *17*, 366–382.
10. Harvey, B.M., Ferri, S., and Orban, G.A. (2017). Comparing Parietal Quantity-Processing Mechanisms between Humans and Macaques. Trends Cogn. Sci. *21*, 779–793.
11. Tsouli, A., Harvey, B.M., Hofstetter, S., Cai, Y., van der Smagt, M.J., Te Pas, S.F., and Dumoulin, S.O. (2022). The role of neural tuning in quantity perception. Trends Cogn. Sci. *26*, 11–24.
12. Nieder, A., Freedman, D.J., and Miller, E.K. (2002). Representation of the quantity of visual items in the primate prefrontal cortex. Science *297*, 1708–1711.
13. Nieder, A., and Miller, E.K. (2003). Coding of cognitive magnitude: Compressed scaling of numerical information in the primate prefrontal cortex. Neuron *37*, 149–157.
14. Viswanathan, P., and Nieder, A. (2015). Differential impact of behavioral relevance on quantity coding in primate frontal and parietal neurons. Curr. Biol. *25*, 1259–1269.
15. Eiselt, A.K., and Nieder, A. (2016). Single-cell coding of sensory, spatial and numerical magnitudes in primate prefrontal, premotor and cingulate motor cortices. Exp. Brain Res. *234*, 241–254.
16. Ramirez-Cardenas, A., Moskaleva, M., and Nieder, A. (2016). Neuronal Representation of Numerosity Zero in the Primate Parieto-Frontal Number Network. Curr. Biol. *26*, 1285–1294.
17. Viswanathan, P., and Nieder, A. (2020). Spatial Neuronal Integration Supports a Global Representation of Visual Numerosity in Primate Association Cortices. J. Cogn. Neurosci. *32*, 1184–1197.
18. Viswanathan, P., Stein, A.M., and Nieder, A. (2024). Sequential neuronal processing of number values, abstract decision, and action in the primate prefrontal cortex. PLoS Biol. *22*, e3002520.
19. Nieder, A., and Miller, E.K. (2004). A parieto-frontal network for visual numerical information in the monkey. Proc. Natl. Acad. Sci. USA *101*, 7457–7462.
20. Viswanathan, P., and Nieder, A. (2013). Neuronal correlates of a visual "sense of number" in primate parietal and prefrontal cortices. Proc. Natl. Acad. Sci. USA *110*, 11187–11192.
21. Jacob, S.N., and Nieder, A. (2014). Complementary roles for primate frontal and parietal cortex in guarding working memory from distractor stimuli. Neuron *83*, 226–237.
22. Machts, T., Grüb, J., and Nieder, A. (2025). Neuronal encoding of recognition memory for numerical quantities in macaque intraparietal and prefrontal cortices. Prog. Neurobiol. *251*, 102794.
23. Chafee, M.V., and Goldman-Rakic, P.S. (2000). Inactivation of parietal and prefrontal cortex reveals interdependence of neural activity during memory-guided saccades. J. Neurophysiol. *83*, 1550–1566.
24. Oguchi, M., and Sakagami, M. (2022). Dissecting the Prefrontal Network With Pathway-Selective Manipulation in the Macaque Brain-A Review. Front. Neurosci. *16*, 917407.
25. Buschman, T.J., and Miller, E.K. (2007). Top-down versus bottom-up control of attention in the prefrontal and posterior parietal cortices. Science *315*, 1860–1862.
26. Salazar, R.F., Dotson, N.M., Bressler, S.L., and Gray, C.M. (2012). Content-specific fronto-parietal synchronization during visual working memory. Science *338*, 1097–1100.
27. Pesaran, B., Nelson, M.J., and Andersen, R.A. (2008). Free choice activates a decision circuit between frontal and parietal cortex. Nature *453*, 406–409.
28. Gregoriou, G.G., Gotts, S.J., Zhou, H., and Desimone, R. (2009). High-frequency, long-range coupling between prefrontal and visual cortex during attention. Science *324*, 1207–1210.
29. Dotson, N.M., Salazar, R.F., and Gray, C.M. (2014). Frontoparietal correlation dynamics reveal interplay between integration and segregation during visual working memory. J. Neurosci. *34*, 13600–13613.
30. Crowe, D.A., Goodwin, S.J., Blackman, R.K., Sakellaridi, S., Sponheim, S.R., MacDonald, A.W., 3rd, and Chafee, M.V. (2013). Prefrontal neurons transmit signals to parietal neurons that reflect executive control of cognition. Nat. Neurosci. *16*, 1484–1491.
31. Semedo, J.D., Jasper, A.I., Zandvakili, A., Krishna, A., Aschner, A., Machens, C.K., Kohn, A., and Yu, B.M. (2022). Feedforward and feedback interactions between visual cortical areas use different population activity patterns. Nat. Commun. *13*, 1099.
32. Merten, K., and Nieder, A. (2009). Compressed scaling of abstract numerosity representations in adult humans and monkeys. J. Cogn. Neurosci. *21*, 333–346.
33. Jannasch, L.L., Grüb, J., and Nieder, A. (2025). Shared cognitive biases influence numerical judgments in macaques and crows. Proc. Natl. Acad. Sci. USA *122*, e2512219122.
34. Tudusciuc, O., and Nieder, A. (2009). Contributions of primate prefrontal and posterior parietal cortices to length and numerosity representation. J. Neurophysiol. *101*, 2984–2994.
35. Jacob, S.N., Hähnke, D., and Nieder, A. (2018). Structuring of Abstract Working Memory Content by Fronto-parietal Synchrony in Primate Cortex. Neuron *99*, 588–597.e5.
36. Merchant, H., Crowe, D.A., Robertson, M.S., Fortes, A.F., and Georgopoulos, A.P. (2011). Top-down spatial categorization signal from prefrontal to posterior parietal cortex in the primate. Front. Syst. Neurosci. *5*, 69.
37. Christophel, T.B., Klink, P.C., Spitzer, B., Roelfsema, P.R., and Haynes, J.D. (2017). The Distributed Nature of Working Memory. Trends Cogn. Sci. *21*, 111–124.

38. Genovesio, A., Wise, S.P., and Passingham, R.E. (2014). Prefrontal-parietal function: from foraging to foresight. Trends Cogn. Sci. *18*, 72–81.

39. Rosenberg-Lee, M., Ashkenazi, S., Chen, T., Young, C.B., Geary, D.C., and Menon, V. (2015). Brain hyper-connectivity and operation-specific deficits during arithmetic problem solving in children with developmental dyscalculia. Dev. Sci. *18*, 351–372.

40. Estévez-Pérez, N., Sanabria-Díaz, G., Castro-Cañizares, D., Reigosa-Crespo, V., and Melie-García, L. (2023). Anatomical connectivity in children with developmental dyscalculia: A graph theory study. Prog. Brain Res. *282*, 17–47.

41. Michels, L., O'Gorman, R., and Kucian, K. (2018). Functional hyperconnectivity vanishes in children with developmental dyscalculia after numerical intervention. Dev. Cogn. Neurosci. *30*, 291–303.

42. Schwizer Ashkenazi, S., McCaskey, U., O'Gorman Tuura, R., and Kucian, K. (2025). Altered Effective Connectivity of the Numerical Brain in Children With Developmental Dyscalculia. J. Neurosci. Res. *103*, e70066.

43. Kuhl, U., Sobotta, S., and Legascreen Consortium; and Skeide, M.A. (2021). Mathematical learning deficits originate in early childhood from atypical development of a frontoparietal brain network. PLoS Biol. *19*, e3001407.

44. Galvin, V.C., Yang, S.T., Paspalas, C.D., Yang, Y., Jin, L.E., Datta, D., Morozov, Y.M., Lightbourne, T.C., Lowet, A.S., Rakic, P., et al. (2020). Muscarinic M1 Receptors Modulate Working Memory Performance and Activity via KCNQ Potassium Channels in the Primate Prefrontal Cortex. Neuron *106*, 649–661.e4.

45. Goldman-Rakic, P.S., Muly, E.C., 3rd, and Williams, G.V. (2000). D(1) receptors in prefrontal cells and circuits. Brain Res. Rev. *31*, 295–301.

46. Arnsten, A.F.T. (2011). Catecholamine influences on dorsolateral prefrontal cortical networks. Biol. Psychiatry *69*, e89–e99.

47. Ott, T., and Nieder, A. (2019). Dopamine and Cognitive Control in Prefrontal Cortex. Trends Cogn. Sci. *23*, 213–234.

48. Kutter, E.F., Bostroem, J., Elger, C.E., Mormann, F., and Nieder, A. (2018). Single Neurons in the Human Brain Encode Numbers. Neuron *100*, 753–761.e4.

49. Kutter, E.F., Dehnen, G., Borger, V., Surges, R., Mormann, F., and Nieder, A. (2023). Distinct neuronal representation of small and large numbers in the human medial temporal lobe. Nat. Hum. Behav. *7*, 1998–2007.

50. Kutter, E.F., Dehnen, G., Borger, V., Surges, R., Nieder, A., and Mormann, F. (2024). Single-neuron representation of nonsymbolic and symbolic number zero in the human medial temporal lobe. Curr. Biol. *34*, 4794–4802.e3.

STAR★METHODS

KEY RESOURCES TABLE

REAGENT or RESOURCE	SOURCE	IDENTIFIER
Experimental models: Organisms/strains		
Macaca mulatta	German Primate Center, Göttingen	www.dpz.eu
Software and algorithms		
NIMH Cortex	National Institute of Mental Health	https://www.nimh.nih.gov/labs-at-nimh/research-areas/clinics-and-labs/ln/shn/software-projects.shtml
MAP Data Acquisition System	Plexon	https://plexon.com/
MATLAB R2020b	MathWorks	https://www.mathworks.com
MATLAB code	MathWorks	https://doi.org/10.6084/m9.figshare.31235425

EXPERIMENTAL MODEL AND PARTICIPANT DETAILS

Subjects

Two male adult rhesus monkeys (*Macaca mulatta*) were implanted with two recording chambers each, centered over the principal sulcus in the dorsolateral prefrontal cortex (PFC) and the intraparietal sulcus (IPS) in the posterior parietal cortex (monkey 1 and monkey 2, both left hemisphere). Chamber implantation was guided by anatomical magnetic resonance imaging (MRI) and stereotaxic measurements. All surgeries were performed under sterile conditions while the monkeys were under general anesthesia. The monkeys received postoperative antibiotics and analgesics. All procedures were performed in accordance with the guidelines for animal experimentation. All experimental procedures had been ethically reviewed and approved and were regulated and supervised by the national authorities, the Regierungspräsidium Tübingen, Germany.

METHOD DETAILS

Experimental apparatus and stimuli

Monkeys were seated inside primate chairs in a chamber 57 cm away from a 15″ flat screen monitor (with a resolution of 1,024 by 768 pixels and a refresh rate of 75 Hz). The NIMH Cortex software (Bethesda, MD) was used to present the stimuli and behavioral data acquisition. The monkeys' eye gaze was tracked by an infrared eye tracking system (ISCAN, Cambridge, MA).

We used random dot arrays as numerosity stimuli ranging between 1 and 5 dots (diameter range from 0.5° to 0.9° of visual angle). Each unique dot pattern was presented on a gray background circle subtending 5.4° of visual angle and was used as sample and test stimulus. A custom-written MATLAB (The Mathworks, Natick, MA) program generated the stimuli anew before each recording session to prevent the monkeys from memorizing stimulus sequences. Sample and test stimulus of the same countable numerosity were never identical within a trial and session. In order to control for low-level, non-numerical visual features in half of the trials, dot diameters were selected randomly (standard protocol). In the other half of the trials, dot density and total occupied area were equated across stimuli (control protocol). Trials of the standard and control protocol were pseudo-randomly and unpredictably presented.

Behavioral protocol

We trained two macaque monkeys on a modified version of the delayed match-to-numerosity task in which the monkeys had to match test numerosities to sample numerosities (see Machts et al.[20]). Nonmatching numerosities that were presented between sample and matching test stimulus had to be ignored. Up to three sequential numerical nonmatches were presented, i.e., the task consisted of up to three test phases and in each test phase the right or wrong numerosity could occur. A trial was initiated from the monkeys by grabbing a bar and maintaining eye fixation within 3.5° of visual angle of a central white dot. Trials were immediately aborted (blue screen appears) and excluded from further analysis if the animals broke fixation. At first, a gray circular background was shown for 500 ms (pure fixation period). Subsequently, the sample stimulus containing 1 to 4 dots appeared for 600 ms. This sample stimulus had to be memorized over a delay of 1000 ms (again gray background circle) and had to be compared in a following sequence of test numerosities. Each test stimulus was presented for 800 ms with a 100 ms delay between each other. For the case that the numerosity in test stimulus was same as in the sample (match situation, 1–4), monkeys had to respond with a bar release. If the numerosities were different (nonmatch situation, 1–5), the animals continued to hold the bar. A nonmatch numerosity was never shown twice per trial. Sample numerosities and trial types (i.e., if no nonmatch, one nonmatch, two nonmatch or three nonmatch numerosities were

presented) were balanced across conditions and displayed with equal probability (25% each, pseudo-randomly intermixed). Thus, monkeys could not predict when or whether the match stimulus would appear. Correct decision per trial was rewarded with a drop of water. In 25% of the trials, when presenting three nonmatch numerosities in sequence, monkeys were rewarded when holding the bar throughout the whole trial until display-offset. Since the number of trials a monkey can perform during an experimental session is limited (on average monkey 1 completed 483 trials and monkey 2 534 trials), not all possible combinations of sample (1–4) and test numerosities (1–5) could be presented. Therefore, a predefined collection of 64 unique sample-test-combinations was shown.

Neurophysiological recordings

In each session, arrays of up to eight glass-coated 1 MΩ tungsten microelectrodes (Alpha Omega LTD, Israel) were inserted in each recording chamber using custom-made screw microdrives and a grid (Crist Instruments, USA) with 1 mm spacing. To access the IPS, electrodes were passed along the course of it to a depth of 9–10 mm. A MAP Plexon system was used for signal acquisition, amplification, filtering and digitalization. Multi-unit selection was performed offline by adjusting a threshold that separates noise from neuronal activity (Plexon Systems, USA).

QUANTIFICATION AND STATISTICAL ANALYSIS

Data analysis

To focus on network interactions, we analyzed thresholded multi-unit activity (MUA) rather than single-unit activity, using one MUA trace per electrode (up to eight per area). Across 43 sessions, an average of 6.0 ± 0.2 sites were recorded per session in VIP and 6.3 ± 0.2 in dlPFC. Using MUA increases robustness by pooling spikes from multiple neurons per electrode and allowed us to correlate the full population activity between areas for all trials. Electrodes with an average firing rate below 0.5 spikes/s across trials were excluded from subsequent analyses.

All values in the main text and figures refer to the mean ± SEM. SEM was calculated as the standard deviation divided by the square root of the number of samples.

To ensure that our analysis was not contaminated by motor activity, we analyzed the network interactions between PFC and VIP just until the end of the delay period, i.e., the following analyses considered the fixation (500 ms), sample (600 ms) and delay period (1000 ms). We set a criterion of at least 50 recorded trials per correct and error trials, respectively. Furthermore, we used just sessions with at least four intact electrodes per brain area in order to capture robust brain interactions. 43 of 60 sessions fulfilled this criterion (12 sessions from monkey 1, 31 sessions from monkey 2).

Population correlation analysis

The population correlation analysis closely follows the description provided by Semedo et al.[29] However, instead of single-unit activity, we correlated the entire recorded neuronal activity (multi-unit activity) of the inserted electrodes (freed from noise). To capture the relationship between neuronal activity across the two brain areas, we filtered out the 'mean signal' across the trials. To do this, we first z-scored the multi-unit activity and then subtracted the corresponding peri-stimulus time histogram (PSTH), resulting in residual activity. This process was repeated for each electrode separately, without considering the different sample sizes and protocols as individual groups. We then used CCA to identify pairs of dimensions in each brain area such that the correlation between the projected activity onto these dimensions is maximized. This can be described by the following formula:

$$\underset{\boldsymbol{a},\boldsymbol{b}}{\operatorname{argmax}} corr(\boldsymbol{Xa}, \boldsymbol{Yb}),$$

where X is a $n \times p_x$ matrix containing the residual activity of the VIP population, Y is a $n \times p_y$ matrix containing the residual activity of the PFC population, n represents the number of data points, and p_x and p_y are the number of electrodes in each of the two areas. The vectors a and b are one-dimensional and define dimensions in the population activity space of each area. CCA can identify additional pairs of dimensions by searching for vectors that maximize the same correlation, provided they are uncorrelated with the initial pair of canonical variables. However, our CCA identified just one pair of dimensions with significant population correlations, since the correlation values of the second canonical pair were, on average across all tested sessions, around 80% lower (correct trials: 78.1 ± 2.26%; error trials: 76.9 ± 2.45%; N = 43 sessions). Therefore, we only considered the first canonical pair for our analyses.

To measure population correlations at different time points, we defined two time windows with a length of 160 ms in each area. These time windows with the starting times t_1 and t_2 relative to trial onset were slide in 20 ms steps along the trial length. While doing this we additionally shifted both windows against each other with a maximal lag of ±40 ms in 1 ms steps ($d = t_1 - t_2$) to compute population correlations at different lag periods. Thus, defining the time within the trial as $t = t_1$, each entry in the population correlation can described as follows:

$$C(t, d) = P(t, t + d) = \underset{\boldsymbol{a},\boldsymbol{b}}{\max} corr(\boldsymbol{X}_t\boldsymbol{a}, \boldsymbol{Y}_{t+d}\boldsymbol{b}),$$

Due to the relatively small number of trials per recording session (at least 50 trials per group; see above), we counted the spikes in each time window in non-overlapping 20 ms bins. This process resulted in a two-dimensional map containing the population correlation values for each time point and lag period. We created such maps separately for each recording session. To calculate the

population correlation maps for correct and error trials, we balanced the number of trials by setting a common value (50 trials) for each group. This process was repeated 25 times, with a different random subset of trials each time. The average of these 25 maps was taken as the final value for the respective session. Additionally, we calculated a null distribution for each session using the same procedure described above, except that the neuronal activity was shuffled for each area and time window. This process was repeated 500 times, and the resulting shuffled population correlation maps were used for a permutation test to determine whether the population correlation coefficient for each time bin could be explained by chance. The significance threshold was set to $p < 0.05$ (two-sided), meaning that the actual population correlation coefficient had to be greater than 97.5% of the values in the null distribution. We averaged the results across the 43 sessions that met our criteria and displayed the resulting population correlation map as a heatmap.

On the basis of population correlation maps, we computed for each session and each 20 ms time step a feedforward ratio in order to see at which time point the neuronal activity is more driven by a feedforward or feedback signal. The feedforward ratio is defined as follows:

$$Feedforward\ ratio = \frac{(AUC_{\text{feedforward}} - AUC_{\text{feedback}})}{(AUC_{\text{feedforward}} + AUC_{\text{feedback}})},$$ where $AUC_{feedforward}$ is the area under the positive-lag sides (or curve) of the population correlation map and $AUC_{feedback}$ is the area under the negative-lag sides of the population correlation map. By creating a shuffled distribution, we were able to see which ratio was significantly above chance or not. To do this, we eliminated the correspondence whether the calculated population correlation coefficients belong to the negative or positive lag. We performed this process 500 times and for each time bin separately. The significance threshold was set to $p < 0.05$ (two-sided). Furthermore, we compared the AUC values for the positive and negative lags between the correct and error trials by using a two-sided Wilcoxon signed-rank test. Analogous to what was described above, we used the shuffled distribution of population correlation maps to create a significance threshold ($p < 0.05$, two-sided).

Finally, we calculated mean population correlation functions which refer to the average of all population correlation functions across the time lags between the brain areas (−40 ms till +40 ms). These functions were constructed for correct and error trials und compared by a two-sided Wilcoxon signed-rank test. For visualization, the differences between the functions were plotted.

Centroid-based lag estimation

To characterize the temporal structure of inter-areal correlations, we quantified the lag at which canonical correlations peaked for each time bin during correct trials. For each bin, the lag of the maximum CCA value was identified from the time-lagged correlation matrix. To assess the robustness of these lag estimates, we computed a centroid around each peak, defined as the range of lag values encompassing the 95th percentile of CCA values centered on the maximum. The centroid provides a measure of the temporal spread of the correlation peak and was used for visualization. All analyses used the same preprocessing and CCA parameters as in the main analyses.

Population correlation analysis for specific neuronal populations

To examine the contribution of numerosity-selective neuronal populations to inter-areal communication, we repeated the canonical correlation analysis after stratifying multi-unit activity (MUA) by task selectivity. MUAs were classified as sample-selective, delay-selective, or non-selective based on numerosity tuning during the sample and/or delay period, using the same criteria as our single-unit analyses (one-way ANOVA, factor numerosity, $p < 0.01$; see Machts et al.[20]). Neuronal responses during the sample period were quantified in a 600-ms window, shifted 100 ms after sample onset to account for typical visual response latency. Delay-period activity was analyzed in a 1000-ms window, shifted 100 ms after sample offset.

All recording sessions included in the main correct/error trial analyses were also used here. However, stratifying by selectivity reduces the number of available MUAs per class. Therefore, the analysis required a minimum of one MUA per cortical area (VIP and dlPFC) and selectivity class per session, rather than the four-MUA minimum used in the main analyses.

MUAs selective during both sample and delay periods were included in both the sample- and delay-selective groups. Using this criterion, heatmaps of time-lagged CCA values were constructed from 43 sessions: 29 sessions with non-selective MUAs, 38 with sample-selective MUAs, and 40 with delay-selective MUAs. Apart from the adjusted inclusion criterion, the CCA procedure, preprocessing, and statistical analyses were identical to those in the main analyses.